On detecting kissing bonds in adhesively bonded joints using electric time domain reflectometry

Philip Johannes STEINBILD [1], Robin HÖHNE [1], René FÜßEL [1], Niels MODLER [1]
[1] TU Dresden, Institut für Leichtbau und Kunststofftechnik,
Holbeinstr. 3, 01307 Dresden, Germany

Contact e-mail: philip_johannes.steinbild@tu-dresden.de

Abstract. The use of fibre reinforced plastics to achieve low mass aircrafts calls for suitable joining technologies. The joining technology with the highest potential in lightweight construction with fibre reinforced plastics is adhesive bonding. However, in today's aircrafts the potential of adhesive bonding is limited due to the additional use of rivets as crack arrestors for regulation and safety issues. To meet the regulations and reduce the number of joint-weakening, heavy rivets, an adhesive bond needs to be monitored during its production and throughout its lifetime in operation. State of the art are ultrasound and thermal imaging technologies for non-destructive testing of adhesive bonds. The use of such technologies in a structural health management system is not practical. Additionally, ultrasound and thermal imaging technologies are only capable of detecting gross defects like areas of uncured adhesive and voids. The detection of adhesion defects like kissing bonds still pose a serious problem. This paper describes a novel adhesive sensor principle based on the electric time domain reflectometry, which can detect differences in the deformation of the adherents in an adhesively bonded joint under load to infer that a kissing bond is taking effect. The sensor is integrated into the joint. Results of the experimental validation by shear tension testing of single lap shear specimens with the adhesive sensor integrated into the joint are presented. The deformation of the adherents is monitored by digital image correlation and compared to the data obtained by the electric time domain reflectometry. The results show that by integrating the proposed sensor into an adhesively bonded joint the joint can be monitored operando. This novel technology can be used in a structural health management system to raise the confidence in adhesive bonds and reduce the number of rivets thus reducing mass. Further developments will include the use of a finite difference time domain model to numerically test sensor configurations regarding its geometry and electrical properties.

1. Introduction

The increasing use of composite design and fibre reinforced plastics (FRP) in the aerospace industry calls for suitable lightweight joining technologies. The joining technology featuring the highest lightweight potential is the adhesively bonded joint. The adhesively bonded joint enables transferring forces through low tension over large areas of the joint without using additional high-mass joining elements like screws or rivets. Especially the use in joining FRP parts is advantageous because continuous fibres are not damages by the joining process [1].

Incorrect manufacturing can lead to defects, which lower the carrying capacity of the adhesive joint drastically. The defects can also induce cracks into the joint, causing failure. One of the challenges is the prevention of interfacial weak bonds like kissing bonds. The relatively small dimensions of interfacial weak bonds make a detection via non-destructive testing (NDT) difficult [2]. This paper gives an insight on the detection and surveillance of kissing bonds using the difference in deformation of the adhesive joint at and around the defect. A novel sensor principle based on the electric time domain reflectometry (ETDR) is presented and experimentally investigated.

2. State of the Art

2.1 Kissing Bond

A kissing bond, also known as zero volume debond, is an interfacial weakness between adhesive and adherent. The kissing bond is a region in the adhesive bond in which the adhesive could not or only to certain extend establish adhesion while curing. Thus, the adhesive and the adherent are only partly joined or adhesive and adherent are touching but no forces can be transferred [2-6]. Figure 1 shows a schematic diagram of a kissing bond.

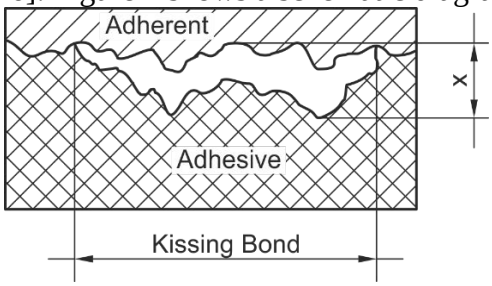

Fig. 1. Schematic diagram of a kissing bond.

A typical reason for a kissing bond is a not or insufficiently cleaned adherent surface which is still contaminated e.g. by a release agent or oil used in the manufacturing process of the adherent.

The detection of kissing bonds via conventional NDT like advanced ultrasonics or radiographic techniques are few and still subject of interest. The defects introduced in the adhesive bond are as small as nanometres (thickness ***x*** in Fig. 1). The mentioned conventional NDT detect differences in transmission properties of the bond. Since the kissing bond is a small defect, the effect on the transmission properties are too small to be detected in most cases [6].

The detectability of a kissing bond under load via digital image correlation (DIC) has been evaluated in [5]. Single lap shear samples made of glass fiber reinforced plastics (GFRP) as adherents and epoxy resin as the adhesive layer containing varied areas of kissing bond were examined under shear load. The kissing bond was introduced by placing an ethylene-tetraflourethylen-copolymer (ETFE) based release film on the adhesive surface before the actual joining process. The results showed different strain on the outer surface of an adherent in areas with kissing bond compared to those without kissing bond [5].

2.2 Electric Time Domain Reflectometry

The ETDR method is well-established in the electrical industry to analyse transmission lines. Based on run time and characteristics of reflections the ETDR method allows the space-resolved measurement of electric signals fed into transmission lines such as coaxial cables. A transmission line consist in the most basic case of two conductors with a dielectric layer in between (Fig. 2).

Maxwell's equations are the mathematical basis for describing the propagation of electromagnetic waves. Assuming only transverse electromagnetic (TEM) waves or quasi TEM waves exist in a certain transmission line, the calculation of the electromagnetic properties can be done by applying the transmission theory. Rather than calculating the field strengths ***E*** and ***H***, the transmission theory allows the calculation of the transmission properties ***I*** and ***U*** without the need to determine the electromagnetic field by use of Maxwell's equations. This allows determining the propagation of electromagnetic waves by solely analysing the geometry of the transmission line. The derivation of the transmission theory is based on the assumption that the electric and magnetic field structures in the transverse plane are identical to the stationary field structures at direct current excitation. The conformity of the field structures allow the definition of the transmission line properties ***I*** and ***U*** as well as the derivation of an equivalent circuit diagram through the method of describing stationary fields [9].

A basic transmission line and the corresponding equivalent circuit diagram are shown in Figure 2.

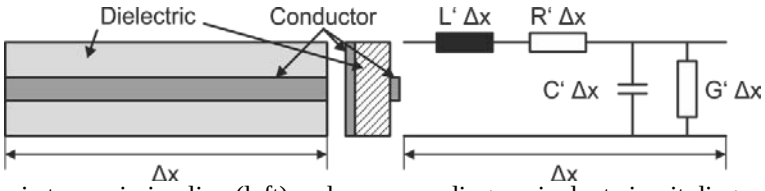

Fig. 2. Basic transmission line (left) and corresponding equivalent circuit diagram (right).

The properties of the transmission line show in Figure 2 can be described by the properties resistance, inductance, lateral conductivity, and capacity per unit length ***R'***, ***L'***, ***G'***, and ***C'*** respectively. One of the properties of a transmission line is the characteristic impedance Z_0. When excited by alternate or pulsed current the characteristic impedance is calculated by equation 2.1 [10].

$$Z_0 = \sqrt{\frac{R' + j\omega L'}{G' + j\omega C'}} \tag{2.1}$$

For high frequencies or pulsed current ***R'*** and ***G'*** are negligibly small compared to the frequency dependent quantities ***C'*** and ***L'***. Assuming small loss or lossless transmission lines, ***R' = G' = 0*** which leads to (2.2) in which ***a*** represents the width of the conductors, ***b*** the distance between the conductors, μ the magnetic permeability, and ε permittivity [10].

$$Z_0 = \sqrt{\frac{L'}{C'}} = \sqrt{\frac{b^2 \mu}{a^2 \varepsilon}} \tag{2.2}$$

The mentioned reflections in an ETDR measurement are induced by the change of electric properties of the transmission line. Since the characteristic impedance Z_0 depends on the basic electric properties inductance per unit length ***L'*** and capacity per unit length ***C'***, a change in ***L'*** or ***C'*** leads to a change in the characteristic impedance of the transmission line.

The ETDR method relies on a high frequency signal being fed into the transmission line. For this, an impulse generator is needed to generate the high frequency signal. To be able to measure the reflections an oscilloscope is also needed. The ETDR measurement device used in this paper is the D-TDR 3000 by Sympuls Aachen, shown in Figure 3 (right). It combines both devices needed for an ETDR measurement into one compact device. The equivalent circuit diagram in Figure 3 (left) shows the configuration of both, impulse generator and oscilloscope.

To perform measurements of the reflections in a transmission line, the investigated transmission line is connected to an ETDR measurement device via a coaxial cable. The outer and inner conductor is connected to one of the conductors of the transmission line respectively. The impulse generator sends repeating wave signals through the transmission line. At a change in impedance in the transmission, part of the wave is reflected while the remaining part keeps going through the transmission line. When the partly reflected signal

reaches the oscilloscope, the location of the change in impedance can be determined by means of runtime and phase velocity. The phase velocity v_p complies with (2.3), with ε_0 electric constant, ε_r .relative permittivity, μ_0 magnetic constant, and μ_r relative permeability.

$$v_p = \frac{1}{\sqrt{L'C'}} = \frac{1}{\sqrt{\varepsilon_0 \varepsilon_r \mu_0 \mu_r}} \tag{2.3}$$

To outline the impedance over the course of the transmission line it is necessary to calculate the impedance after every change in impedance ***i***.

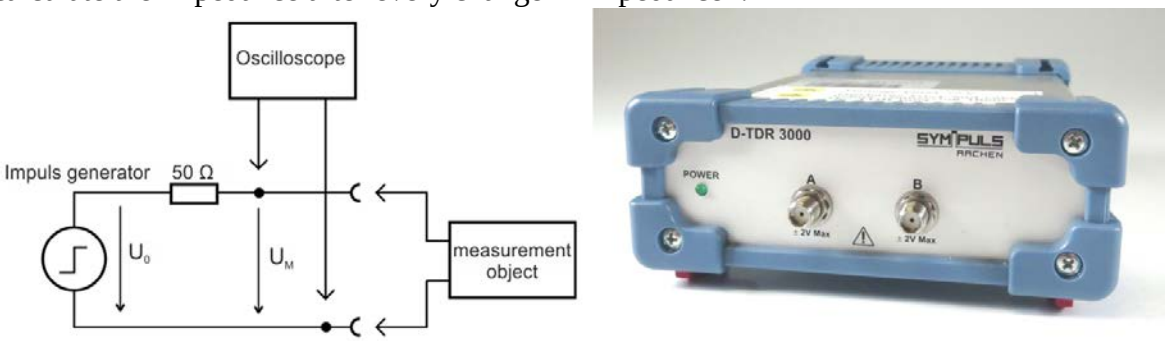

Fig. 3. ETDR measuring device D-TDR 3000 by Sympuls Aachen (right) and the corresponding equivalent circuit diagram (left) [11].

The reflection coefficient Γ decribes the ratio of the reflected (V_{ref}) to the incoming voltage amplitude (V_{inc}) and can be determined via the ratio of the impedances before (Z_{pre}) and after the change in impedance (Z_{after}) (2.4) [12].

$$\Gamma = \frac{V_{ref}}{V_{inc}} = \frac{(Z_{after} - Z_{pre})}{(Z_{after} + Z_{pre})} \tag{2.4}$$

For $i = 1$ Γ is calculated by means of (2.4). For $i > 1$ Γ corresponds to (2.5) [13].

$$\Gamma_i = \frac{\Delta V_i}{V_i \prod_{k=1}^{i-1}(1-\Gamma_k)} \tag{2.5}$$

ΔV_i represents the difference in voltage amplitude at the change of impedance i and V_i the voltage amplitude before the change of impedance i. V_i corresponds to (2.6) [13].

$$V_i = (1 + \Gamma_{i-1}) \cdot V_{i-1} \tag{2.6}$$

The impedance after the change of impedance i, Z_i, corresponds to (2.7) [13].

$$Z_i = Z_{i-1} \frac{(1+\Gamma_i)}{(1-\Gamma_i)} \tag{2.7}$$

The characteristic impedances from (2.7) plotted over the runtime give the characteristic impedance curve. In practice, the characteristic impedance curve is not calculated but measured at the undamaged object and used as a reference for further measurement.

The spatial or rather the time resolution of the ETDR measuring device depends on the rise time of the impulse signal. An infinitely high resolution is only possible in theory when the voltage can be built up in $t_R = 0$ s. Since this is not possible in practice, consecutive reflections are only distinguishable when the distance between them is at least the distance which the impulse signal travels in half of the rise time t_R [14].

Since the 1950s, ETDR is being used in energy and communication industry to detect imperfections in various cables. In the 1970s, the technology was adapted for geotechnology applications [15]. In geotechnology ETDR is mainly used for determining the relative permittivity or conductivity in a probing or for failure detection. The relative permittivity and conductivity of geotechnically relevant materials give information about their properties like moisture content while sudden changes in the electrical properties might indicate collapsed mine shafts [16].

In the 1990s, ETDR was developed further for structural health monitoring of concrete beams. Lin et. al. developed a method to detect and quantify strains and cracks in concrete beams [17]. Further developments used an elastomer as a dielectric to enhance the sensitivity of the sensor for strain [13].

Höhne et. al. developed a sensor principle for the distributed detection of strains by means of carbon fibre which shows very high sensitivity to strain in 2016 [18].

For the characterisation of crack propagation in fibre reinforced plastics Abu Obaid et. al. 2005 used an ETDR method and achieved a resolution of up to 0.3 mm [19].

ETDR and electrical frequency domain reflectometry (EFDR) measurements on adhesively bonded joints were first described in [7]. Samples using aluminium adherents and various polymer adhesives were examined. The relative permittivity of the polymers were calculated and compared using the results obtained by ETDR and electric frequency domain reflectometry (EFDR). Furthermore, the investigations showed that the time domain signals changed when the geometry was altered due to differences in joint thickness [7]. In [8] the influence of humidity and aging on adhesively bonded joints using ETDR was investigated.

These investigations confirm the applicability of ETDR for adhesively bonded joints. However, in adhesively bonded joints only the overall behaviour of the ETDR signals were considered. To allow the use of ETDR methods for structural health monitoring of adhesively bonded joints a novel sensor principle is presented and investigated in this paper.

3. Sensor Principle and Experimental Setup

Vijaya Kumar et. al. suggest that the monitoring of axial strain of the adherents can be used to detect kissing bonds in adhesively bonded joints [5]. The deformation of the adherents under load differs in damaged and undamaged areas of the joint when affected by kissing bonds. This forms the basis for the proposed sensor principle described in this paper.

The proposed sensor principle is shown in Figure 4. The sensor itself consists of an upper (red) and a lower (green) conductor. The adhesive acts as a dielectric between the upper and lower conductor. The conductors are connected to an ETDR measuring device, which measures the spatial impedance of the pair. In the unloaded condition (Fig. 4, left), the conductors cover each other completely. This delivers an impedance of $\boldsymbol{Z_{w0}}$ in the transmission line over the width of the sensor thus the adhesive bond. When the bond is loaded (Fig. 4, right), the kissing bond in area II causes the upper adherent to behave differently in area II than in area I. The difference in deformation is transferred to the upper conductor. The measurement shows higher impedances in area II ($\boldsymbol{Z_{w2}}$) than in area I ($\boldsymbol{Z_{w1}}$). Also, impedances in area I are smaller than in the unloaded state.

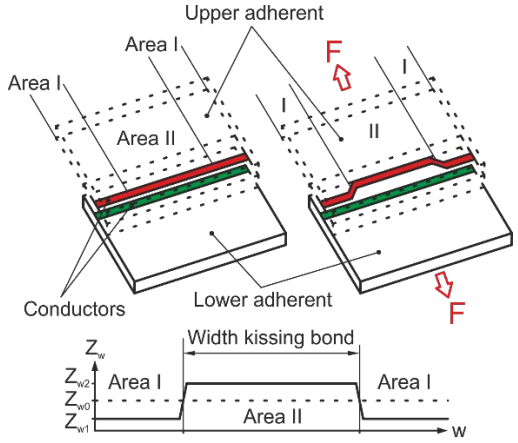

Fig. 4. Proposed sensor principle detecting kissing bonds in area II via ETDR.

This electrical behaviour correlates with the mechanical behaviour. Since there is no adhesion in area II, no lateral contraction of the adhesive occurs in this area. This causes the distance between the two conductors to increase in area II while it decreases in area I. The lateral contraction is overlaid with the difference in deformation of the adherent, respectively the conductor that leads to a characteristic distribution of impedance, Figure 4, bottom.

For the experimental validation single lap shear specimens with an integrated ETDR sensor were used. The adherents were made of the GFRP laminate Polydet® PowerStar having a thickness of 3.3 mm with bidirectional (BD) E-glass as reinforcement fibre and unsaturated polyester (UP) as a matrix. The structural adhesive DOW® Betaforce 2850 based on polyurethane (PUR) was used. The flat conductors were made of shielding 3M Scotch® 1181 (width 3 mm, thickness 0.1 mm). The overall thickness of the joint is 8.6 mm while the thickness of the adhesive is 2 mm, respectively 1.8 mm between the conductors. The adhesive surfaces of the adherents were prepared for joining by sandblasting before applying the flat conductors. The kissing bond was introduced by tape Airtech Flashbreaker® 1 with a thickness of 55 µm. The kissing bond was introduced in the middle of the adhesive surface over the full length of the adhesive surface and a defined width. The adherents were bonded in a bonding tool to maintain a uniform bonding thickness and cured at room temperature for 60 min. The tested specimen configurations are displayed in Table 1.

Table 1. Single lap shear specimens with integrated ETDR sensors used for experimental tests

Specimen ID	Adhesive surface	Kissing bond width
SLS_1	200 × 25 mm²	100 mm
SLS_2	200 × 25 mm²	50 mm

For the ETDR measurements a time domain reflectometer Sympuls D-TDR 3000 was used. The reflectometer and the sensor were connected via a coaxial cable RG-174/U. The inner and outer conductor of the coax were soldered to the upper and lower conductor respectively. A matched termination resistor connect both conductors on the other end of the sensor. A speckle pattern for DIC measurements was applied to the adherent with the induced kissing bond. A single lap shear specimen with integrated ETDR adhesive sensor, soldered coax, termination resistor, and speckle pattern is shown in Figure 5. To make the arrangement of the conductors clear, a cross section of the specimen is also given in Figure 5.

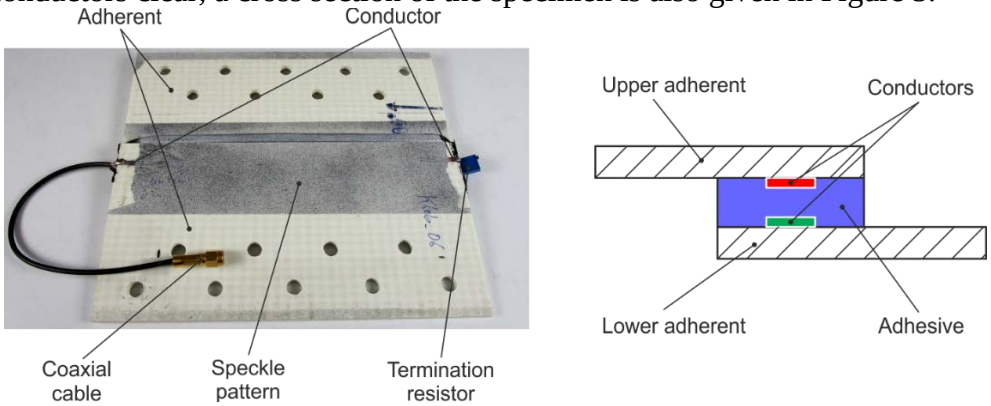

Fig. 5. Single lap shear specimen for experimental validation of the proposed sensor (left) and schematic cross section of the specimen showing the conductor arrangement.

Measurements used for the calculation of a DIC were taken to monitor strain on the outer surface of the kissing bond affected adherent to confirm that the tape introduced kissing bond lowers the carrying capacity of the adhesive bond during the tensile shear test. The data for the calculation of the DIC was measured by the 3D movement and deformation measurement system GOM ARAMIS. A single lap shear specimen with integrated ETDR adhesive sensor was mounted to the universal testing machine Zwick Roell UPM 1465 so that the ARAMIS system can observe the kissing bond affected adherent with applied speckle pattern. The test setup is shown in Figure 6.

4. Experimental Results and Discussion

The strain fields on the adherents outer surfaces obtained by DIC show that kissing bonds were successfully introduced by tape to every specimen. Figure 7 shows the calculated DIC

of both specimens at a displacement of 2.2 mm. The projected area of the surface on which a kissing bond was induced by tape shows no significant strain while the undamaged areas right and left of the damaged area show strain as high as 0.3 %.

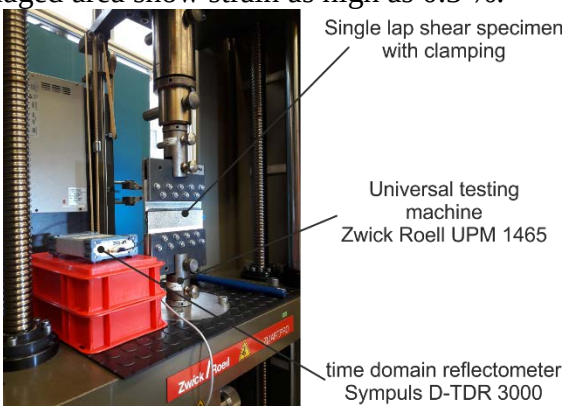

Fig. 6. Test setup for experimental validation of the proposed sensor.

The impedance is referred to the resistance of the termination resistor (50 Ω). The spatially resolved relative impedances over the width of the sensor, respectively the width of the adhesive bond, are shown in Figure 8 for both types of specimens at the unloaded state (0.0 mm) and for a displacement of 2.2 mm.

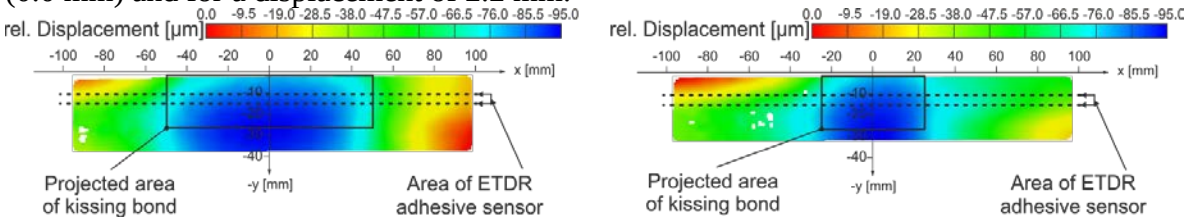

Fig. 7. DIC of specimen SLS_1 (left) and SLS_2 (right) at a displacement of 2.2 mm.

At the transition from the coaxial cable to the sensor at 0 mm a peak indicates big reflections caused by the soldering. At 200 mm the transition from the sensor to the termination resistor takes place, indicated by a smooth rise of the relative impedance. Between those two distinctive points the relative impedances of the sensing transmission line are plotted.

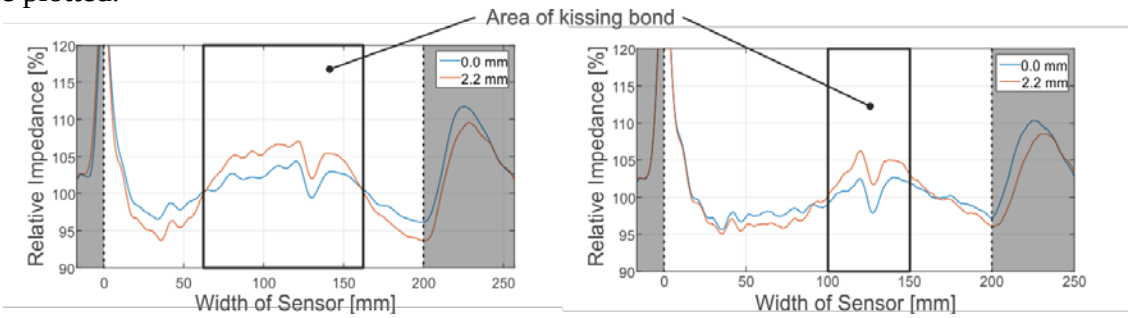

Fig. 8. ETDR impedance signals of specimen SLS_1 (left) and SLS_2 (right) at a displacement of 0.0 mm and 2.2 mm

The level of impedance in the kissing bond affected area is about 2.5 % higher under load than unloaded. In the area with no kissing bond the level of impedance is about 2.5 % lower under load than at no load caused by the lateral contraction of the adhesive. This behaviour can be observed for kissing bonds induced by tape for both widths, 100 mm and 50 mm. Since the dielectric properties of the sensors transmission line change drastically in the area of the kissing bond, the data shows a shift to the right of the sensor, indicating that the kissing bond is not located in the middle. The DIC however showed that the kissing bonds are in fact located in the middle of the specimens. This effect needs to be analysed and compensated in further investigations. The observed behaviour confirms the principle presented in Figure 4.

5. Summary and Conclusion

As shown in the state of the art, conventional NDT methods are not suitable for monitoring adhesively bonded structures operando. Since the sensor solution presented in this paper is integrated in the bonding, it can be used as part of a structural health monitoring system in the future to monitor the carrying capacity of the adhesive bond. In addition, the used measuring equipment to acquire ETDR signals is by far not as high cost as conventional NDT methods.

The adhesive sensor is able to detect adhesive defects like kissing bonds. This function has been experimentally validated. For the experimental validation tensile shear tests using single lap shear specimens with integrated transmission lines as a sensor were manufactured. The DIC calculations for outer adherent surfaces showed that kissing bonds can be prepared by an adhesive tape. ETDR measurements of the integrated transmission lines show different levels of impedances in kissing bond affected and non-kissing bond affected parts of single lap shear specimens, detecting kissing bonds under load.

The ETDR adhesive sensor has the potential to increase the confidence in adhesive bonds in particular and in lightweight structures generally.

References

[1] Schürmann, H.: Konstruieren mit Faser-Kunststoff-Verbunden. 2nd edition. Berlin, Heidelberg: Springer-Verlag, 2007. – ISBN 978-3-540-72189-5

[2] Nagy, P. B.: Ultrasonic Classification of Imperfect Interfaces. In: Journal of Nondestructive Evaluation, vol. 11 (1992), no. 3/4, pp. 127-139

[3] Najib, M. and Nobari, A.: Kissing bond detection in structural adhesive joints using nonlinear dynamic characteristics. In: International Journal of Adhesion & Adhesives, vol. 63 (2015), pp. 46-56

[4] Yan, D.; Neild, S.; Drinkwater, B.: Modelling and measurement of the nonlinear behaviour of kissing bonds in adhesive joints. In: NDT&E International, vol. 47 (2012), pp. 18-25

[5] Vijaya Kumar, R.; Bhat, M.; Murthy, C. R. L.: Evaluation of kissing bond in composite adhesive lap joints using digital image correlation: Preliminary studies. In: International Journal of Adhesion & Adhesives, vol. 42 (2013), pp. 60-68

[6] Jeenjitkaew, C. and Guild, F.: The analysis of kissing bonds in adhesive joints, vol. 75 (2017), pp. 101-107

[7] Li, Z.-C.; Joshi, S.; Hayward, D.; Gilmore, R.; Pethrick, R.: High frequency electrical measurements of adhesive bonded structures: An investigation of model parallel plate waveguide structures. In: NDT&E International, vol. 30 (1997), no. 3, pp. 151-161

[8]Affrossman, S.; Banks, W.; Hayward, D.; Pethrick, R.: Non-destructive examination of adhesively bonded structures using dielectric techniques: Review and some results. In: Proceedings of the Institution of Mechanical Engineers, vol. 214 (2000), pp. 87-102

[9] Paul, C. C.: Analysis of multiconductor transmission lines. Hoboken, New Jersey: John Wiley & Sons, Inc., 2008. – ISBN 978-0470131541

[10] IPC-2141A: Design Guide for High-Speed Controlled Impedance Circuit Boards. Northbrook, IL: IPC – Association Connecting Electronics Industries, 03.2004

[11] Sympuls – Gesellschaft für Pulstechnik und Messsysteme mbH: Wellenwiderstandsmessgerät D-TDR 3000: Gerätehandbuch. Aachen, 2014.

[12] Liao, S. Y.: Microwave Devices and Circuits: Third Edition. Englewood Cliffs, NJ: Prentice Hall, 1996

[13] Lin, M. W.; Thaduri, J.; Abatan, A.: Development of an electrical time domain reflectometry (ETDR) distributed strain sensor. In: Measurement Science and Technology, vol. 16 (2005), pp. 1495-1505

[14] Tektronix Inc.: TDR Impedance Measurements: A Foundation for Signal Integrity. 2007

[15] Chen, G.; Mu, H.; Pommerenke, D.; Drewniak, J. L.: Damage Detection of Reinforced Concrete Beams with Novel Distributed Crack/Strain Sensors. In: Structural Health Monitoring, vol. 3 (2004), no. 3, pp. 225-243

[16] Benson, C. H. and Bosscher, P. J.: Time-Domain Reflectometry (TDR) in Geotechnics: A Review. In: Nondestructive and Automated Testing for Soil and Rock Properties. ASTM STP 1350 (1999), pp. 113-136

[17] Lin, M. W.; Abatan, A.; Zhang, W.-M.: Crack damage detection of concrete structures using distributed electrical time domain reflectometry (ETDR) sensors. In: Proceedings of SPIE Conference on Smart Systems for Bridges, Structures, and Highways 3671 (1999), pp. 297-304

[18] Höhne, R.; Ehrig, T.; Kostka, P.; Modler, N.: Phenomenological investigation of a carbon fibre based strain sensor with spatial resolution by means of time domain reflectometry. In: Materialwissenschaft und Werkstofftechnik, vol. 47 (2016), no. 11, pp. 1024-1033
[19] Abu Obaid, A.; Yarlagadda, S.; Yoon, M. K.; Hager III, N. E.; Domszy, R. C.: A Time-domain Reflectometry Method for Automated Measurement of Crack Propagation in Composites during Mode I DCB Testing. In: Journal of Composite Materials, vol. 40 (2006), no. 22, pp. 2047-2066